Homogeneous Pin-Through-Hole Component Inspection Using Fringe Tracking

K. Sundaraj
University Malaysia Perlis (UniMAP)
School of Mechatronics Engineering
02600 Jejawi - Perlis
MALAYSIA
kenneth@unimap.edu.my

Abstract: - Automated visual inspection (AVI) systems are playing important roles in ensuring manufacturing quality in the electronic industry especially in the assemblage of printed circuit boards (PCB). Most existing AVIs that are used for PCB inspection are categorized as non-contact inspection systems consisting of a single overhead camera. Such systems, which can be manual or automated, are incapable of detecting 3D pin-through-hole (PTH) component placement defects and reporting them. By considering an assembled PCB as a textured surface with a predefined depth map, we propose to apply an angled fringe projection to detect defects in PTH component placement. It has been found that angled fringe projection can be used for surface analysis by applying phase shifting and phase unwrapping obtained from several images. However, the turnover time for PCB inspection is very crucial in the electronic industry. In other words, an alternative improved method that speeds up the inspection process is always desirable. This paper describes a method of applying an angled fringe projection for 3D height measurement using a single captured image and a direct triangulation technique. The main focus of this paper has been made on the development of a fringe tracking algorithm and its practical implementation details. This algorithm allows us to obtain the depth map of the surface under analysis with just one image. The simulated data and calibration process of the tracking algorithm are discussed and an experimental result is given for Peripheral Component Interconnect (PCI) component insertion in computer motherboards. With proper system calibration and accurate image processing, we demonstrate the successful manipulation of a structured collimated light source for height measurement using a single captured image.

Key-Words: - Automated Visual Inspection, Fringe Projection, PCB Inspection.

1 Introduction

Inspection has long been an integral part of quality control in many industries ranging from agricultural to the high-end electronic industry. The process of determining if a product deviates from a given set of specification is defined as inspection. Inspection involves measurement of specific part features such as surface finishing and geometric dimensions [1]. Human inspectors have been predominantly carrying out these visual inspection tasks in most industries. However, requirements of the modern manufacturing environment have intensified the usage of automated visual inspection (AVI) systems (also known as automated optical inspection (AOI) systems). The main reason for the demand of machine vision systems in modern manufacturing is the trend towards total quality that is products with zero defects [2] and to improve the planning and controlling of component assembly [3].

In the electronic industry, total quality control coupled with the evolution of high dense PCB boards is pushing human inspectors to their limits. AVIs seem to be the best choice to replace human inspectors. A number of research groups have done work in the individual areas of hardware and software application of 2D and 3D AVIs. Both [4] and [5] describe work done using a single spot laser beam. A triangulation technique is used to obtain range values. The major drawback with this method is that only one range value per frame can be obtained at any one time. In [6] the development of a 3D inspection system for surface mount device (SMD) assemblies that is reliable and inexpensive is presented. The inspection operation presented in their paper consists of detecting the presence and absence of components. This system utilizes a sheet-of-light triangulation technique, whereby the circuit board is illuminated with a laser. The geometric properties of the system are utilized to calculate the height values from each reflected sheet-of-light. [7] utilizes a wavelet-based image difference algorithm to locate 2D defective areas in PCBs. A coarse resolution defect localization algorithm is proposed. This algorithm will map the defective areas found in the coarse differenced image to the fine resolution of the tested image. Another localization algorithm presented in [8] uses an histogram distribution graph coupled with the summing of pixel frequencies over a chosen range of gray values. The limitation of the gray-scaled image caused some problem when applied to certain colored components. The work presented in [9] and [10] used the image differencing technique to detect defects using blocks of images representing various parts of a PCB. A similar approach is presented in [11] whereby the authors introduce the application of neural networks and fuzzy logic in image blocks or sub images of a printed circuit board. In [12] color image processing with multi-lighting techniques were used to detect different type of defects in different types of components. Colored lights were switched on and off depending on the type of inspection performed. [13] and [14] used a similar method for the inspection of solder joints in their work. An investigation into the use of optical fibers and other light guides for the inspection of solder joints between pin grid arrays and printed wire boards was done in [15]. An efficiency rate of 92% was reported in this work. Matrix and vector based image processing techniques on 2D images of PCBs were carried out in [16] and [17]. Another vector based method based on connectivity points and edge detection to locate tracks on PCBs is presented in [18].

However, the previously mentioned works concentrate on horizontal defects and do not address specifically the problems posed by PTH components. Human operators usually inspect these components because their defects are *invisible* in a 2D image. The types of components in this category include electrolyte capacitors, edge-connectors, Universal Serial Bus (USB) ports and PCI connectors as shown in Fig. 1. PTH components are placed manually by human operators and the protruding leads are then soldered below the PCB. The soldering process can be manually done by an operator or by a wave machine that heats molten solder. Defects in PTH components can occur during the placement, soldering or inspection process especially when humans are involved in either of these processes. Unlike defects that have been considered previously like horizontal misalignment, missing component, wrong component or bad solder joints, PTH components pose a completely different problem; tilt. Component tilt can be considered as the vertical misalignment of a component. An image provided by an overhead camera will not be able to detect this misalignment. It is interesting to note that according to [19] and [20], tilt of components is a one of the major problem in the manual assembly area. PTH components are usually loose fit and hence easily tilted. When these components travel on a soldering machine conveyor, they are prone to jerk which causes tilt. Apart from this, other factors that cause tilt are due to environment conditions that induce the operators to insert the components wrongly. These errors, according to the authors, render assembly lines that have components manually inserted unreliable. It is claimed that such lines have a high customer-defect-return rate. The average defect level of PTH components is around 1000 parts-per-million (ppm) and can go as high as 4000 ppm.

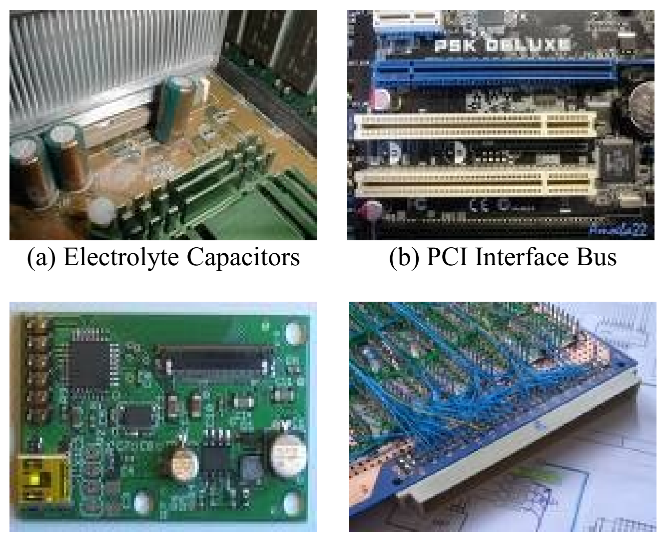

(a) Electrolyte Capacitors (b) PCI Interface Bus

(c) USB Serial Port (d) 64-Pin Connector

Figure 1. PTH components that are found on a typical computer motherboard.

This paper presents an alternative technique in image processing to perform surface analysis. While the previous approaches process 2D images to localize horizontal defects, very few have used fringe projection to detect vertical misalignments of PTH components. The application of fringe projection for surface analysis is not new. The work in [21] analyses the application of digital filtering in the calculation of height measurement from fringe patterns. In [22] fringe projection is used for edge detection of objects.

However, the proposed technique could only be applied when the object and background are homogeneous. The work presented in [23] tracked the shape of moving objects using fringe projection and laser tracking. In [24] an algorithm that improves the phase unwrapping process by using a type of quality map is proposed for the acquisition of dense 3D surfaces. A similar work [25] uses fringe contrast to improve the phase unwrapping process. The study of bacterial growth has been carried out using fringe projection in [26]. In [27] a unified analysis in the analysis of phase distortion is presented. Our method also uses the familiar fringe projection approach in the calculation of height measurement from fringe patterns. On the other hand, we differ from other approaches in this category whereby we only need a single image after the calibration process in order to computer the depth map of the surface under analysis. We apply neither phase shifting nor need phase unwrapping to compute the height values. This can be attributed to the development of a robust fringe-tracking algorithm that is focus of this paper. We also present the calibration procedures and the details about the practical implementation of our method that is crucial in order to obtain accurate results. Simulation results of the proposed tracking algorithm will be discussed and its limitations presented. We apply our fringe-tracking algorithm in an experiment carried out for PCI component insertion in computer motherboards.

2 Principle of Operation

Fringe projection techniques can be used to measure the surface height of an object [28] [29]. The detailed information of the surface profile is contained in the observed change in fringe patterns. Consider a structurally coded light that is projected on an object placed in a background. When this fringe is viewed from a different angle, the fringe pattern appears shifted on the surface of the object. Fig. 2 shows the case when the object is viewed normal to the surface of the background. Because of the difference in the viewing angle θ and object height h, the fringe pattern has moved from point X to X'. This shift δx is equivalent to a phase-shift $\delta\phi$ where,

$$\delta\phi = 2\pi \frac{\delta x}{\lambda} \qquad (1)$$

and λ is the length of the fringe pattern. To obtain the absolute surface height profile using fringe projection, we propose to calculate the distance δx, between the break of a ray on the surface and on the flat background as shown in Fig. 2. A point to note with regards to the projected fringe is that the source of projection has be a collimated light source in order to have constant θ along the surface under inspection. Otherwise the wavelength of the fringe λ will vary along the background surface. In this case, additional work must be done to calibrate the values of θ and λ with respect to surface location.

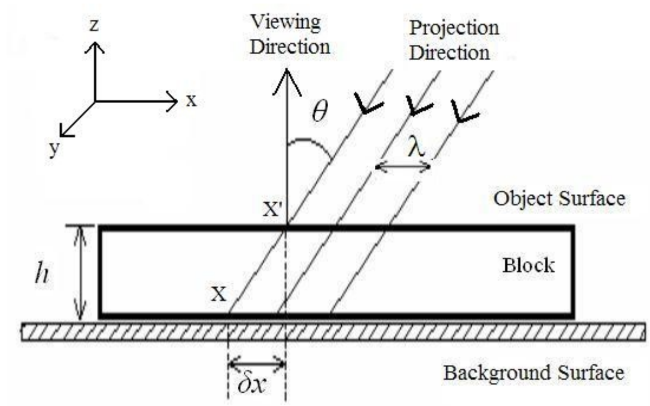

Figure 2. Fringe projection illuminating a block surface.

Once a collimated light source is used to project a fringe onto the surface under analysis, calculation of the fringe shift δx will enable the computation of the height of the block h at a specific location given by the triangulation equation,

$$h = \frac{\delta x}{\tan\theta} \qquad (2)$$

where θ is the angle of projection of the collimated light which is known from the experiment setup. Fig. 3 shows a sample image of undeformed and deformed fringe pattern obtained from an object and background of homogeneous surface. In the case when the object and background have surfaces that are non-homogeneous the computation of δx is not straightforward. The reflection of the fringe pattern onto non-uniform textured surfaces will produce images of shifted fringe patterns that are not identical to those of that in the background. A classical solution to this problem is fringe projection with phase shifting and phase unwrapping. This method has been extensively used by researchers in many applications.

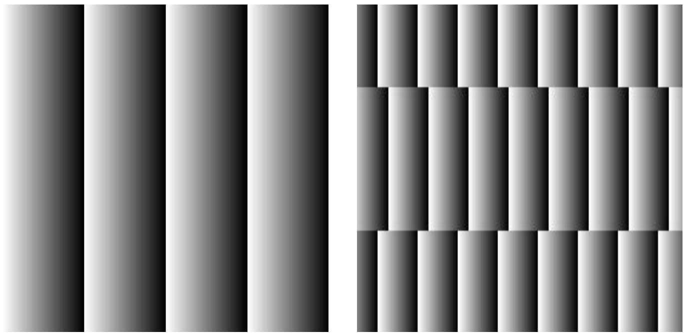

(a) (b)

Figure 3. (a) Undeformed and (b) deformed fringe patterns.

Let us consider a general modulated fringe pattern at pixel location *(i,j)* given by,

$$I_{(i,j)} = A_{(i,j)} + B_{(i,j)} W[\ldots]_{(i,j)} \tag{3}$$

where A and B are illumination constants and the function W is given by,

$$W[\ldots]_{(i,j)} = f(\phi, \varphi, \omega) \tag{4}$$

where ϕ, φ and ω are the modulation parameter, modulation shift and modulation frequency respectively at pixel location *(i,j)*. Most researches use sinusoidally-coded structured light with the phase angle as the modulation parameter. In such a case, the general equation representing the fringe is given by,

$$I_{(i,j)} = A_{(i,j)} + B_{(i,j)} \cos\left[\phi_{(i,j)} + \delta\phi_{(i,j)}\right] \tag{5}$$

where, by shifting the fringe patterns in three stages of 0, $2\pi/3$ and $4\pi/3$, three simultaneous equations can be obtained for the three unknowns (A, B and ϕ). These equations can then be solved by various phase unwrapping algorithms to obtain the solution for $\delta\phi$. Accuracy of the method can be improved by shifting the fringe patterns in an increased number of stages. However, this leads to complex phase unwrapping functions. In [30] a recurrent method is presented to solve such functions. Unfortunately, according to [31] phase unwrapping algorithms can be very inaccurate and very long execution times are often involved.

In order to do away with the phase shifting and phase unwrapping problems to speed up the inspection process, we propose to use a robust fringe-tracking algorithm. By tracking the fringe pattern as it moves from X to X' as shown in Fig. 2, we are able to compute δx in order to determine the height measurement. To do this, we note that the fringe position at X is actually the image of the captured fringe pattern on the background surface with the camera is along the z-axis and the projector positioned at an angle θ along the xz-plane. This image, which is called the reference fringe image, must be obtained during the calibration process in a situation where the background surface is homogeneous and defect free. If now a PTH component is placed on the background, the camera would see a movement in the fringe pattern. This image is called the shifted fringe image. The computation of the shift δx obtained from the two images is done using the fringe-tracking algorithm performed by the host computer.

In our algorithm, we use a method to track similar pixel values column wise. Pixel values in both images are modeled using equation (3). However, since we are comparing intensity values in the reference and shifted images, it is not necessary to explicitly determine the values of $A_{(i,j)}$, $B_{(i,j)}$ or $\phi_{(i,j)}$. The determination of δx will be sufficient to obtain h from equation (2). Consider a particular pixel at row i and column j denoted as *(i,j)*. If pixel intensity at *(i,j)* of the shifted image is equal to the reference intensity of column j, then $\delta x_{(i,j)}$ is zero. Otherwise a search is done to the neighboring right or left columns along the same row to find a match. The direction of search is determined from the angle of projection. If a match is found v pixels away, then $\delta x_{(i,j)}$ is proportional to v. The next pixel in that column is then processed until all pixels in the image have been completed. The pseudo code for these steps is given in Algorithm 1. We would like to note here that the proposed algorithm is dependent on the fringe pattern. In our case a simple fringe obtained from a saw-tooth periodic function is used.

The effect of noise on the accuracy of δx was investigated by increasing the standard deviation σ of the Gaussian noise in the simulated images. In this experiment, an object of rectangular shape with color that is homogeneous with the background is simulated at the center of the image. Pixel location *(i,j)*, was used as the modulating parameter of the W function. The modulation frequency f, was varied but fringe pitch λ, was kept constant. The rectangular object with varying height h, was simulated by changing the modulation shift ϕ, at predefined locations. In these experiments, row $i=0$ is used to provide the reference values for each column j. The computed $\delta x_{(i,j)}$ was recorded in a depth map and is stored as an image. The results are shown in Fig. 4 where it can be seen that by using a suitable W function, the fringe tracking algorithm is resilient to noise as given by a low detection error rate, e. Unfortunately, the proposed algorithm has a well-defined limitation when applied to our selected fringe pattern (periodic saw-tooth). Given a certain illumination angle θ and fringe pitch λ, there exists a certain maximum height h_{max} that can be measured. It is given by,

$$h_{\max} = \frac{\lambda}{\tan\theta} \tag{6}$$

Algorithm 1. Fringe Tracking Algorithm

```
R = Total number of image rows
C = Total number of image columns
I^j_ref = Reference intensity level at column j
I_(i,j) = Shifted intensity level at pixel location (i,j)
δx_(i,j) = Height variation at pixel location (i,j)
for j = 0 to C do
    for i = 0 to R do
        if I_(i,j) = = I^j_ref then
            δx_(i,j) = 0
        else
            v = 0
            while j + v < C || j + v > 0 do
                if I_(i,j) = = I^j_ref then
                    STOP
                else
                    v++ || v--
                end if
            end while
            δx_(i,j) = v
        end if
    end for
end for
```

In other words, by assuming the maximum variation in height measurement for the surface under test, we have to adjust the illumination angle θ and the modulation frequency of the projected fringe pattern ω before the experiment such that equation (6) is satisfied at all times.

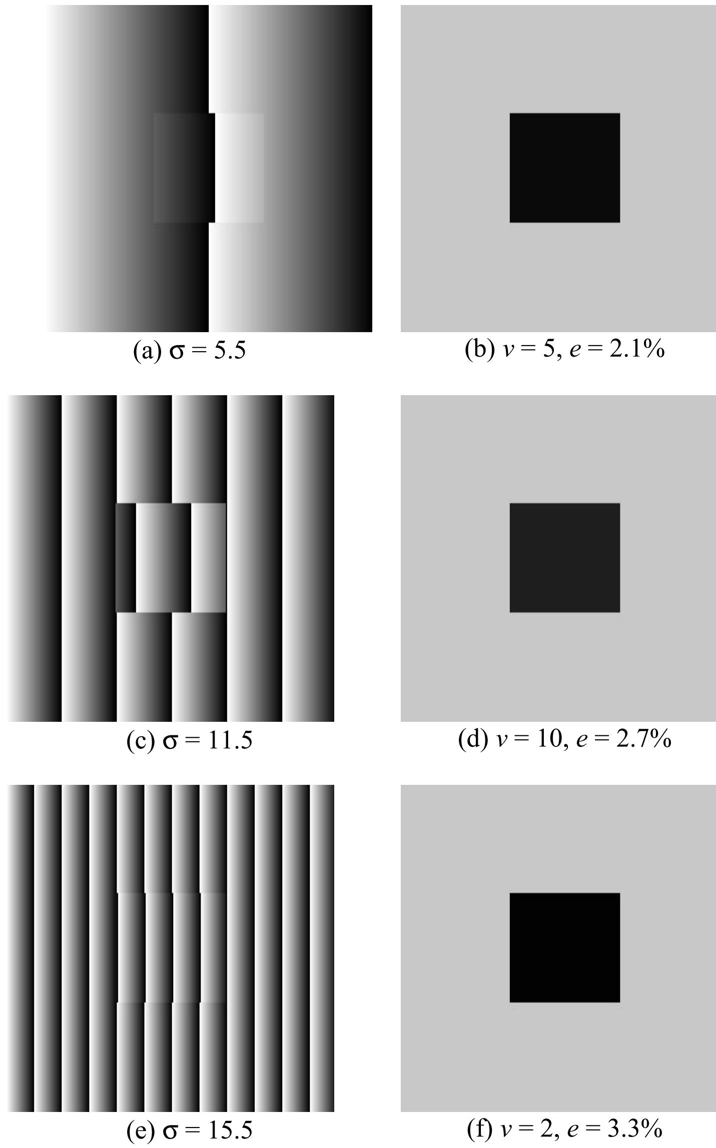

Figure 4. Simulation of 3D surface using a saw-tooth fringe pattern with various standard deviation of Gaussian noise σ, modulation frequency ω and a rectangular object with various heights h. The deformed fringe patterns are shown in (a), (c) & (e). The computed depth maps with the accuracy rate are shown in (b), (d) & (f). The depth map reveals the exact location of the simulated rectangular object computed by the fringe tracking algorithm in the presence of noise.

3 Calibration and Implementation

In order to implement the fringe tracking algorithm a systematic calibration process must be adopted. To understand the rational behind the steps, we must first understand the basic processes in the inspection of a PCB in the electronic industry. Before each assembled board is processed, there is always a master board which is carefully assembled and ensured to be defect free. This master board will provide the default values to the AVI system during inspection. During inspection, an incoming PCB will be clamped down, fixed and then moved horizontally such that various critical sections of the PCB are captured by the overhead camera. This camera has the capability to zoom in on any particular area of interest that has been predetermined by the programmer. Once the images have been captured, they are processed against similar images that were obtained using the master board. Any significant deviation in the analysis will render that particular location of the board as defective. In some AVI systems a detailed report will be generated for each board stating all defective areas.

The first step in our calibration process requires the reference fringe image to be captured for a particular PCB. This is a gray scale image of the predetermined projected fringe pattern. This can be obtained from an empty PCB of white color. Such a particular PCB can be requested from the manufacturer. Generally manufacturers of PCBs comply with requests from inspection sub-contractors to ensure marketability of their boards. Given such a board, the reference fringe pattern can be easily obtained for various critical section of the board once the projector and camera has been installed in the AVI system. This fringe pattern corresponds to the height at datum level.

The next step in the calibration process is to determine *fringe quality*. This is done by measuring the standard deviation σ of the Gaussian noise that is present in the image of the captured fringe pattern. In our implementation, we did a column wise (σ_j) and row wise (σ_i) intensity pixel check for several known predetermined fringe patterns. These fringe patterns vary by 256 levels for a distance of one wave-length λ occupied by 256 pixels. Our aim was to quantify the error in the pixel values as we go down each column and across each row. The results of these experiments are shown in Table 1. Another experiment was done to determine the average difference in horizontal and vertical pixel intensity values between the computer generated fringe pattern and the captured fringe pattern. The results of these experiments are shown in Table 2. There is no particular explanation to quantify this error as this strongly depends on the reflective properties of the areas surrounding the board, type of camera and projector but these values can help us determine a suitable W function.

Table 1. Average horizontal and vertical standard deviation of noise in the captured image.

Fringe Pattern	σ_i	σ_j
Sine	7.8	3.4
Saw-Tooth	4.2	3.2
Quadratic	10.3	3.1
Random	3.1	3.3

Table 2. Average horizontal and vertical standard deviation of noise between the computer generated image and captured image.

Fringe Pattern	$\Delta\sigma_i$	$\Delta\sigma_j$
Sine	10.1	8.6
Saw-Tooth	6.4	6.2
Quadratic	12.3	10.3
Random	7.8	5.9

A third important issue that is important in the implementation is the determination of the resolution of inspection. Fringe patterns that are computer generated vary in intensity levels at pixel level which is about 0.25mm depending on the graphics hardware. It is necessary to measure the fringe pitch λ after projection on the PCB and the number of pixels V, that correspond to a one wave-length on the captured image. Height measurement can then be determined during inspection using,

$$h = \frac{v}{V} \cdot \frac{\lambda}{\tan\theta} \tag{7}$$

where v is the result from the fringe tracking algorithm. The average length between one intensity level and the next intensity level as measured from the projected fringe pattern on the PCB will determine the minimum resolution of measurement that can be made. This is shown in Figure 5.

Another important issue in the calibration process is the choice of fringe pattern. This is determined by the W function. This is probably the most crucial part that determines the success or failure of the algorithm. As shown in Table 1, four types of fringe patterns were projected onto the PCB. In order to successfully track the fringe, the intensity levels in the fringe must be as distinct as possible. From Table 1, it can be seen that the intensity levels for a particular column in the fringe do not differ much with an average of 3.25 among all fringe pattern. The same cannot be said about the variation row wise. In other words, although any function can be used to computer generate the fringe pattern, we have to make sure that successive intensity values within one wave-length must be greater than σ_i.

$$\left| I_{(i,j+1)} - I_{(i,j)} \right| > \sigma_i \ \forall \ (i, j) \tag{8}$$

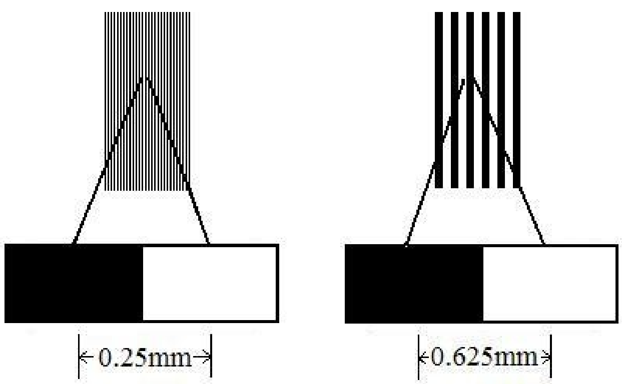

(a) Computer generated fringe pattern

(b) Measured value on the PCB of the projected fringe

Figure 5. Determination of minimum spatial resolution of measurement.

Figure 6 shows the four fringe patterns that have been generated with at least $\sigma_i > 15$. As we have mentioned before, our choice of fringe pattern is the saw-tooth pattern. We chose this because the tracking algorithm was easier to be implemented for this fringe pattern. Also based on our hardware, experimental setup and fringe coding, this pattern produced the lowest average of (σ_i, σ_j, $\Delta\sigma_i$, $\Delta\sigma_j$). An advantage in the inspection of PTH components is that not all pixels in the surface under analysis need to be processed. For a PIC connector for example, a speed up can be obtained by just checking the four corners of the component and the center line of the component. For an electrolyte capacitor, a minimum of three points on the radius of the capacitor spaced at 120° apart plus the center is required. From a practical point of view, inspection of these pixels alone is sufficient to provide information on the vertical alignment of the PTH component. A last important point to note is the color of the surface of the PTH component. Since the reference fringe pattern has been obtained by using a white PCB, the component also has to have an homogeneous white surface. As we have mentioned before, once the feasibility of a particular technique for inspection has been established, it will be possible to standardize the surface color of certain components according to the requirements of the AVI systems. Such color coding standardization can then be sent to component manufacturers to be incorporated in their production line. In our experiments, all the PCI connectors used had white homogeneous surface color.

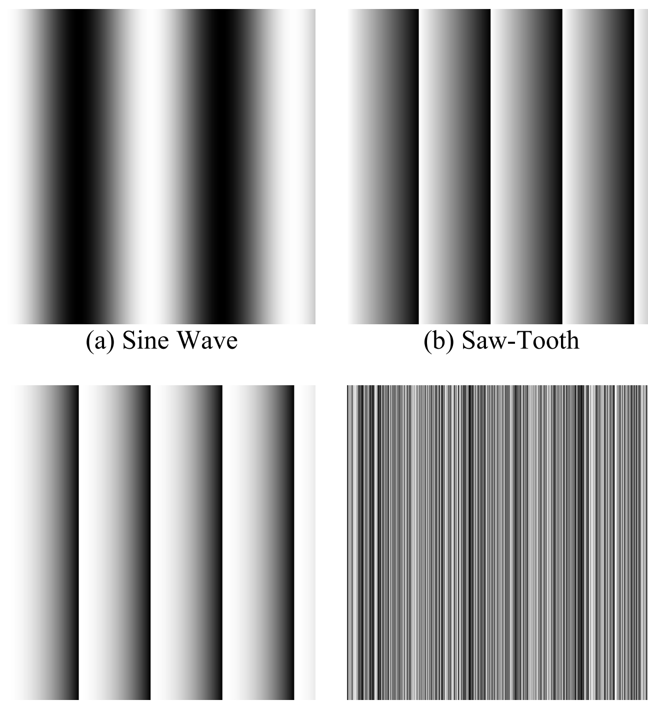

(a) Sine Wave (b) Saw-Tooth

(c) Quadratic (d) Random

Figure 6. Four different forms of carefully generated waveforms considering the noise factor from the setup.

4 Experimental Setup and Results

An experimental setup was devised to simulate a standard PCI connector of a computer motherboard. Fig. 7 shows the experimental setup used in this work. This setup was done on a rigid optical table. Alignments and right-angle determination was made by using water levelers. The liquid crystal display (LCD) projector was placed overhead normal to the surface under test. The digital CCD camera used was a

Marlin FO33C progressive scan with a macro zoom lens. It was however placed at a particular angle to the surface under test to give the required field of view (FOV). This was to simulate an industry AVI system. The computer used was a Pentium IV 1.8 GHz PC operating under a Windows XP environment to capture and process the incoming frames. The image processing software was programmed using Microsoft Visual C++ 6.0. All triggering and synchronizing of cameras were hardware controlled. The lighting conditions in this setup were however hand controlled.

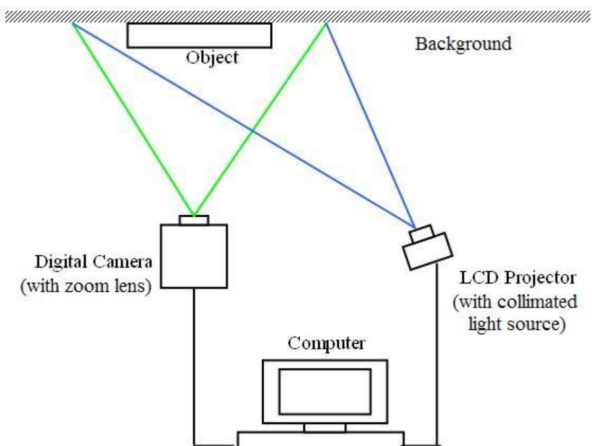

Figure 7. Experimental setup for PTH component defect analysis on a PCB.

Fig. 8 shows a PCB of a computer motherboard that has a PTH component (PCI connector) that has been placed in a defective manner. In a typical AVI system, this defect would have gone unnoticed as the image from the system would have indicated the absence of tilt in the PCI connector as shown in Fig. 8-a. Fig. 8-b shows the side-view of the PCB to highlight this condition. The previously mentioned calibration processes were conducted and a saw-tooth fringe pattern was projected on the PCI and fringe tracking was performed. The image captured by the camera and the results of the 3D height measurement are shown in Fig. 9.

The first point to note is the irregularities in Fig. 9-a and Fig. 9-b. Some of the pixels that belong to a particular column have odd values that deviate from a normal shift of a periodic saw-tooth fringe pattern. This abnormality can be due to some manufacturing defect that has appeared on the surface of the PCB and PCI. Fig. 9-c, 9-d and 9-e show the value of v at each location (i,j) of the PCI connector surface. The absolute variation in height h can then be obtained directly using equation (7) since the illumination angle θ is known from the experimental setup.

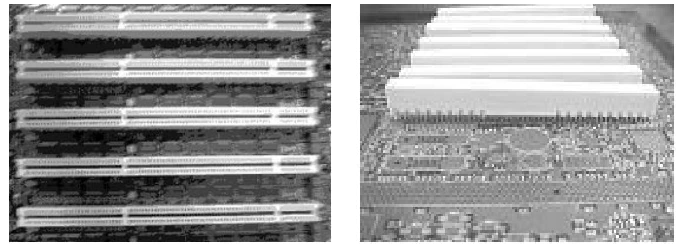

(a) (b)

Figure 8. (a) Plan view of connectors seen directly overhead from current AVI system. Tilt cannot be detected. (b) Side view of connectors. Tilt is noticeable.

We have compared the finally computed height measurement values with measurements obtained from manual inspection using an industrial laser measurement system (LMS). A standard deviation of about 0.6mm was obtained. In Fig. 9-d, we can see that several locations at the bottom right of the image to have some variations in height. This should not be the case as these areas are considered flat. The reason for this discrepancy could be from the fact that the fringe pattern was not projected vertically. Some small skew of several pixels can be observed in Fig. 9-a. This skew has caused a slight variation in the illumination values with respect to the reference values. This is not a serious flaw as industrial AVI systems can be setup to give almost zero skew. Fig. 9-e shows a side view of the computed shift values. We can see clearly that the irregularities are only found in some problematic columns of the image. As mentioned before, we believe these are due to some manufacturing defects present in the surface of the PCI used for the experiment. The time taken to process the image was about 0.2ms for an image size of 320×240 that covered a surface area of about $0.001m^2$ of PCB.

5 Conclusions

This paper shows that it is possible to determine height measurements of an homogeneous surface using a single image with proper image processing using a structured projected fringe pattern. From the simulated images, we have shown that by carefully selecting the modulating function, the generated fringe pattern can be resilient to noise effects. We have also presented the calibration steps and discussed other implementation

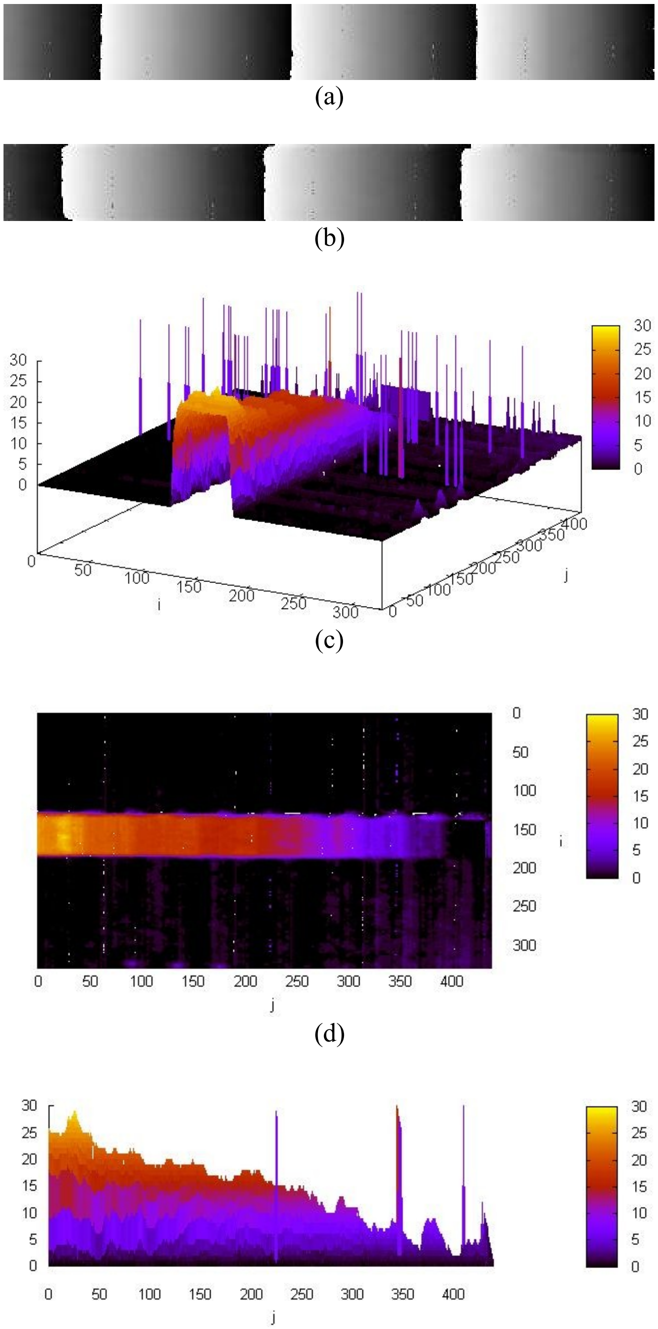

(a) (b) (c) (d) (e)

Figure 9. (a) Reference fringe image captured by the camera at angle θ. (b) Shifted fringe image on PCI component captured by camera. (c) 3D height measurement obtained from Algorithm 1. (d) Top view of the computed depth map. (e) Side view of the computed depth map showing the columns of irregularities.

issues that are crucial to the successful application of the fringe tracking algorithm. From the experimental results done on a defective computer motherboard with a PCI component with vertical misalignment, we have shown that our results are consistent with results obtained using laser measurement systems. The time taken to process an image for a certain surface area of PCB has found to be very low. Hence, the proposed technique can be useful as an inspection method in the electronic industry.

References:

[1] T. S. Newman and A. K. Jain, "A survey of automated visual inspection," *Computer Vision and Image Understanding,* vol. 61, no. 2, pp. 23 1–262, 1995.

[2] M. Moganti, F. Ercal, C. H. Dagli, and S. Tsunekawa, "Automatic PCB inspection algorithms: A survey," *Computer Vision and Image Understanding,* vol. 63, no. 2, pp. 287–3 13, 1996.

[3] K. Salonen, T. Knuutila, M. Johnsson and O. S. Nevalainen. "Planning and Controlling the Component Assembly for Multimodel PCBs," *WSEAS Transactions on Systems*, vol. 5, no. 4, pp. 855-863, 2006.

[4] J. Svetkoff and B. L. Doss, "Automatic inspection of component board using 3D and greyscale vision," *Hybrid Circuits,* pp. 13–18, 1987.

[5] W. Kelley, M. J. Collins, A. A. Jakimcius, and D. J. Svetkoff, "Automatic inspection of SMD printed circuit boards using 3D triangulation," in *International Conference on SME Robots and Vision,* 1988, pp. 33– 47.

[6] E. Guerra and J. R. Villalobos, "A three-dimensional automated visual inspection system for SMT assembly," *Computers in Industrial Engineering,* vol. 40, no. 1-2, pp. 175–190, 2001.

[7] Z. Ibrahim and S. A. R. Al-Attas, "Wavelet-based printed circuit board inspection algorithm," *Integrated Computer-Aided Engineering,* vol. 12, no. 2, pp. 201–213, 2005.

[8] E. K. Teoh, D. P. Mital, B. W. Lee, and L. K. Lee, "An intelligent robotic vision system for inspection of surface mount PCBS," in *IEEE International Conference on Systems and Cybernetics,* 1991, pp. 13–17.

[9] K. Choi, J. Pyun, N. Kim, B. Choi, and S. Ko, "Real time inspection systems for printed circuit

boards," in *Pattern Recognition, Lecture Notes in Computer Science,* 2003, pp. 458–465.

[10] Z. Ibrahim, N. K. Khalid, I. Ibrahim, M. S. Z. Abidin, M. M. Mokji, and S. A. R. S. A. Bakar, "A noise elimination procedure for printed circuit board inspection system," in *AMS '08: Proceedings of the 2008 Second Asia International Conference on Modelling & Simulation (AMS).* Washington, DC, USA: IEEE Computer Society, 2008, pp. 332–337.

[11] M. Moganti and F. Ercal, "A subpattern level inspection system for printed circuit boards," *Computer Vision and Image Understanding,* vol. 70, no. 1, pp. 51–62, 1998.

[12] Kishimoto, N. Kakimori, Y. Yamamoto, Y. Takahashi, T. Harada, Y. Iwata, Y. Shigeyama, and T. Nakao, "A printed circuit board (PCB) inspection system employing the multi-lighting optical system," in *Symposium on Electronic Manufacturing Technology,* 1990, pp. 120– 129.

[13] T. H. Kim, T. H. Cho, S. M. Young, and H. P. Sung, "Visual inspection system for the classification of solder joints," *Pattern Recognition,* vol. 32, no. 4, pp. 565–575, 1999.

[14] W. C. David and E. Sai-Kit, "A tiered-color illumination approach for machine inspection of solder joints," *Pattern Analysis and Machine Intelligence,* vol. 10, no. 3, pp. 387–393, 1988.

[15] A. Kashitani, N. Takanashi, and N. Tagawa, "A solder joint inspection system for surface mounted pin grid arrays," in *Industrial Electronics, Control, and Instrumentation,* 1993, pp. 1865–1870.

[16] E. Whittenberger, A. Brito, and S. Cabrera, "Applying the eigenfaces and fisherfaces methods to circuit board inspection," *Optical Engineering,* vol. 39, no. 12, pp. 3154–3164, 2000.

[17] J. Villalobos, M. Arellano, A. Medina, and F. Aguirre, "Vector classification of SMD images," *Manufacturing Systems,* vol. 22, no. 4, pp. 265–282, 2004.

[18] S. B. Gokturk, L. Akarun, and H. I. Bozma, "Automated inspection of PCBs using a novel approach," in *IEEE workshop on Nonlinear Signal Processing and Image Processing,* 1990, pp. 1865–1870.

[19] S. Oresjo, "A new test strategy for complex printed circuit board assemblies," in *Nepcon,* 1999.

[20] R. N. Sen and P. H. Yeow, "Ergonomic study on the manual component insertion lines for occupational health and safety improvements," *Occupational Safety and Ergonomics,* vol. 9, no. 1, pp. 57–74, 2003.

[21] C. A. Hobson, J. T. Atkinson, and F. Lilley, "The application of digital filtering to phase recovery when surface contouring using fringe projection techniques," *Optics and lasers in engineering,* vol. 27, no. 4, pp. 355–368, 1997.

[22] M. M. Ratnam, "A novel technique for detecting edges in a homogeneous background," in *TENCON,* 2000, pp. 181–186.

[23] S. Tan, D. Song, and L. Zeng, "A tracking fringe method for measuring the shape and position of a swimming fish," *Optics Communications,* vol. 173, no. 1, pp. 123–128, 2000.

[24] C. Diaz and L. Altamirano, "Dense 3D surface acquisition using projected fringe technique," in *ENC '04: Proceedings of the Fifth Mexican International Conference in Computer Science.* Washington, DC, USA: IEEE Computer Society, 2004, pp. 116–123.

[25] L. Chen, C. Quan, C. J. Tay, and Y. Huang, "Fringe contrast-based 3D profilometry using fringe projection," *Optics,* vol. 116, no. 3, pp. 123– 128, 2005.

[26] D. C. Mendez, A. L. Quezada, and M. Lehman, "Fringe projection for the study of bacteriological growth," *WSEAS Transactions on Biology and Biomedicine,* vol. 2, no. 2, pp. 249–252, 2005.

[27] H. Miao, C. Quan, C. J. Tay, and Y. Fu, "Analysis of phase distortion in phase-shifted fringe projection," *Optics and Lasers in Engineering,* vol. 45, no. 2, pp. 318–325, 2007.

[28] S. Yoneyama, Y. Morimoto, M. Fujigaki, and M. Yabe, "Phase-measuring profilometry of moving object without phase-shifting device," *Optics and lasers in engineering,* vol. 40, no. 3, pp. 153–161, 2003.

[29] B. K. Ngoi, K. Venkatakrihnan, N. R. Sivakumar, and T. Bo, "Instantaneous phase shifting arrangement for microstructure profiling of flat surfaces," *Optics Communications,* vol. 190, pp. 109–116, 2001.

[30] K. Abbas, "A two-dimensional recurrent technique for complex functions phase unwrapping," *WSEAS Transactions on Circuits*

and Systems, vol. 5, no. 4, pp. 449–456, 2006.
[31] D. C. Ghiglia and M. D. Pritt, *Two-Dimensional Phase Unwrapping: Theory, Algorithms and Software.* New York Wiley, 1998.